Spiekermann, G., Steele-MacInnis, M., Schmidt, C., Jahn, S. (2012): Vibrational mode frequencies of silica species in SiO2-H2O liquids and glasses from ab initio molecular dynamics. - The Journal of Chemical Physics, 136, 154501-154501-13

DOI: 10.1063/1.3703667

Vibrational mode frequencies of silica species in SiO_2-H_2O liquids and glasses from ab initio molecular dynamics

Georg Spiekermann,[1, a)] Matthew Steele-MacInnis,[2] Christian Schmidt,[1] and Sandro Jahn[1]
[1)] *GFZ German Research Centre for Geosciences, Section 3.3, Telegrafenberg, 14473 Potsdam Germany*
[2)] *Department of Geosciences, Virginia Tech, Blacksburg VA 24061, USA*

(Dated: 22 May 2012)

Vibrational spectroscopy techniques are commonly used to probe the atomic-scale structure of silica species in aqueous solution and hydrous silica glasses. However, unequivocal assignment of individual spectroscopic features to specific vibrational modes is challenging. In this contribution, we establish a connection between experimentally observed vibrational bands and ab initio molecular dynamics (MD) of silica species in solution and in hydrous silica glass. Using the mode-projection approach, we decompose the vibrations of silica species into subspectra resulting from several fundamental structural subunits: The SiO_4 tetrahedron of symmetry T_d, the bridging oxygen (BO) Si-O-Si of symmetry C_{2v}, the geminal oxygen O-Si-O of symmetry C_{2v}, the individual Si-OH stretching and the specific ethane-like symmetric stretching contribution of the $H_6Si_2O_7$ dimer. This allows us to study relevant vibrations of these subunits in any degree of polymerization, from the Q^0 monomer up to the fully polymerized Q^4 tetrahedra. Demonstrating the potential of this approach for supplementing the interpretation of experimental spectra, we compare the calculated frequencies to those extracted from experimental Raman spectra of hydrous silica glasses and silica species in aqeous solution. We discuss observed features such as the double-peaked contribution of the Q^2 tetrahedral symmetric stretch, the individual Si-OH stretching vibrations, the origin of the experimentally observed band at 970 cm^{-1} and the ethane-like vibrational contribution of the $H_6Si_2O_7$ dimer at 870 cm^{-1}.

I. INTRODUCTION

Silicate-bearing aqueous fluids and water-bearing silicate melts play a fundamental role in a wide variety of geologic processes. The structural properties of silica in the presence of H_2O are also of fundamental importance in several scientific and technological areas such as zeolite research and optical glass manufacturing. For these reasons, it is important to understand how the structural properties change with compositions ranging from pure silica to hydrous silica and from dilute silica in aqueous fluids to more concentrated silica solutions.

Much of the current information on the speciation and structure of silica in fluids and in hydrous glasses has come from Raman spectroscopy in the frequency range of 400 to 1200 cm^{-1}, which is dominated by quasi-localized vibrational motions of the silica network.[1–5] A large data set of Raman spectra related to silica species in aqueous fluids at various concentrations is now available.[6–13] The hydrothermal diamond-anvil cell technique[14], in conjunction with Raman spectroscopy, has enabled direct probing of a fluid's vibrational frequencies at high pressures and temperatures. These methods have been applied to silica in predominantly aqueous fluids[2–5,15,16] and water-bearing silicate melts.[3–5,17] Changes in the structure of fused silica glass and binary Na_2O-SiO_2 glasses and melts caused by addition of water have also been investigated by Raman spectroscopy and discussed in terms of silica speciation.[18–23]

Nevertheless, many aspects of the interpretation of Raman spectra of these materials remain uncertain. Ambiguities in the band assignments are mainly the result of the large number of potential species and their different vibrational modes that may be responsible for the observed Raman bands. The possible species include $Si(OH)_4$ monomers, low-order oligomers (dimers, trimers, etc.), more highly polymerized networks of Q^n-species (n denoting the number of oxygen atoms in one tetrahedron shared with neighboring tetrahedra) and deprotonated (charged) species.[2–5,8–10,16] Band assignments are usually based either on qualitative assessment of how spectra change with changing fluid composition, and/or on the results of computational studies of small silicate molecules (see below). Among the Raman bands of silica species in aqueous fluid, the one with the most certain assignment is at about 770 cm^{-1}, which is explained by the tetrahedral symmetric stretch of a monomer.[4,10,15,16,24,25] The agreement on the vibrational frequencies of other monomer modes is fairly good. The case of the dimer is already more ambiguous. All studies agree in its contribution to a band at about 630 cm^{-1} caused by the bridging oxygen vibration, but differ in the frequency of a second band varying from 850 to 915 to 1015 cm^{-1}.[10,15,16,24] Questions remain also about intermediate degrees of polymerization. For instance, the spectral contributions identified for Q^2-species differ markedly between individual studies.[4,5,26,27] Silica rings composed of several SiO_4 tetrahedra (mostly 4 to 6) are important intermediate-range structures, not only in dry silica, but also of silica in solution.[28] Their specific Raman-intense vibrational contribution consists of collective bridging oxygen motions that are referred to as "ring breathing".[29] Their vibrational frequencies are around 600 cm^{-1} and below, a frequency region that is dominated by broad, blurred bands in Raman spectra of silica in solution. Therefore, ring structures are not commonly assigned to Raman bands of silica in aqueous solutions, although NMR measurements detect silica ring structures in these fluids.[28,30]

There are several computational methods to support the interpretation of vibrational spectra from glasses, melts or silica

[a)] georg.spiekermann@gfz-potsdam.de

species in solution. We mention them briefly to motivate the approach presented in this study. They mostly aim to calculate complete Raman spectra of a model system, whereas we aim to study the distinct vibrational contributions of different silica species.

Most commonly, the methodological basis is normal mode analysis (NMA) which explicitly calculates the vibrational modes at zero Kelvin, making use of the harmonic approximation. NMA can be carried out either on clusters or bulk models in periodic boundary conditions. On the basis of the atomic displacement vectors resulting from NMA, several methods have the aim to calculate complete Raman spectra of the modelled system from the polarizability changes related to each mode. For example, the Raman-scattering cross sections are calculated fully ab initio for each vibrational mode of an isolated H_4SiO_4 or $H_3SiO_4^-$ monomer[25,31–33], $H_6Si_2O_7$ dimers and $H_8Si_3O_{10}$ trimers.[16,24,34] In practice, this approach is limited in the size of the silica clusters such that silica species beyond Q^2 have rarely been investigated with gas-phase NMA.[35] Recent advances in the perturbational treatment of polarization within the framework of density-functional theory have allowed calculation of the polarizability tensor of a system within periodic boundary conditions[36] and its variation for finite displacements of the atoms.[37] This method, applied to bulk NMA displacement vectors, allows for the calculation of Raman spectra of bulk disordered silica systems[38,39] in very good agreement with experiment.

A classical approach to calculate polarizability changes of a system due to its vibrations is the parameterized bond-polarizability model. The bond-polarizability model is parameterized based on the polarizability of silica species in crystals[40,41], on ab initio polarizabilities[42–44] or on other electro-optical models.[45] As the above mentioned methods, it can be applied to the atomic displacement vectors of the eigenmodes from NMA.[44]. However, it can also be applied to the atomic velocity vectors of a molecular dynamics trajectory.[42,45] Contrary to the methods above, the bond-polarizability model is suited to disentangle the Raman contributions of different silica Q^n-speciations in partially depolymerized glasses or melts.[40] However, to our knowledge, there is no bond-polarizability model for silica species in hydrous environment.

The goal of our study is to assist the experimental assignment of Raman bands to quasi-local vibrational modes of silica species. Therefore, we need to know the frequencies of vibrational modes with presumably high Raman intensity of distinct silica species. This can not be achieved with the above mentioned methods for silica species of intermediate or high degree of polymerization: If NMA is applied to small clusters as mentioned above, the vibrational character of the modes can be evualuated visually from the atomic displacement vectors of each mode, but in bulk material, this is complicated because of the mixed character of the bulk vibrational eigenmodes.

The approach that is followed in this study is the projection of atomic velocity vectors from ab initio MD runs onto the directions of molecular normal-mode-like motions derived from theoretical spectroscopy. To our knowledge, the first application of this approach were the quasi-normal modes of the water molecule.[46,47] Taraskin and Elliott[48] projected force vectors of bulk classical-potential SiO_2 onto quasi-normal modes of a tetrahedral molecule, to decompose the vibrational density into separate subspectra of different, spatially quasi-localized origin. Wilson and Madden[49] projected atomic velocity vectors from a classical molecular dynamics run of SiO_2 onto the same quasi-normal modes and obtained the partial vibrational density by Fourier transformation of the velocity autocorrelation function. Sarnthein *et al.*[50] used this projection to discover the high frequency doublet of silica to result from two different tetrahedral vibrations as opposed to result from LO-TO-splitting. Pavlatou *et al.*[51] applied the same scheme to a network-forming molten salt in which the polyhedra do not form a complete network. Ribeiro *et al.*[52–54] demonstrated by mode projections in the case of $ZnCl_2$ how the idealized high-frequency quasi-local molecular modes and the idealized low-frequency propagating modes in a network forming liquid are not completely independent of one another. However, the decoupling increases with increasing bond strength.[54] Therefore, the high bond strength of the Si-O bond supports the applicability of local mode projections in silica systems.

Comparison of vibrational subspectra to experimental Raman spectra of silicate glasses and melts is justified by the fact that the first-order Raman scattering shifts of the photon energies directly provide the vibrational frequencies of the scattering species (see e.g. Umari *et al.*[37] and Veithen *et al.*[55]). This contrasts with infrared spectroscopy, in which the complex response to a plane wave radiation field may cause a shift between vibrational frequencies and observed IR absorption bands (see e.g. Balan *et al.*[56]).

This study extends the mode-projection approach to the partially depolymerized network in the SiO_2-H_2O. We present vibrational subspectra from ab initio MD of given silica species. This is reached with the application of the mode-projection approach to molecular subunits comprising 1) silica tetrahedra of any degree of polymerization including the non-polymerized monomer as a benchmark, 2) bridging oxygen atoms to any degree of polymerization, 3) individual Si-OH stretching, 4) O-Si-O vibrations on Q^2-species, and 5) the special ethane-like case of the dimer. The frequencies of these quasi-local modes are compared to the frequencies obtained from Raman spectra and may therefore assist in band assignment. By using bulk MD and extending the mode-projection method, two important limitations of the gas-phase NMA[16,57] are overcome. Firstly, we can model any degree of polymerization. Secondly, silica species in solvation can be modeled at high temperatures[58], including full anharmonicity.

II. METHODS

A. Molecular dynamics simulations

For the calculation of trajectories, we used density functional theory[59] in the plane wave pseudopotential approach, as implemented in the CPMD code.[60] The exchange-correlation

functional was PBE[61], which performs well in hydrous silicates and which has been used in previous studies of the SiO_2-H_2O system.[62,63] Exchange-correlation functionals of the GGA type seem to be generally superior over LDA in disordered network-forming systems.[64–67] We used Martins-Troullier type pseudopotentials.[68] The Kohn-Sham wavefunctions were expanded at the Γ-point only with a plane wave cutoff energy of 80 Ry. Dependence of forces on k-point sampling was negligibly small (below 1%). Tests against higher cutoff energies showed that with the pseudopotentials used, all forces were within about 1% deviation from converged value. This rather high cutoff ensures high reliability of the modeled properties and structures. We used Car-Parrinello (CP) molecular dynamics[69] with a ficticious electronic mass of 400 a.u. and a time step of 4 a.u. (0.097 fs). We found this setting to reproduce the Born-Oppenheimer forces very accurately even after long CP runs. Wavefunctions evolving with combinations of larger mass and time step introduce a non-negligible effect on dynamics and thus on vibrational frequencies.[70–72] The CP fictitious kinetic energy of the wavefunctions was thermostatted. The atomic positions and velocities were recorded every 40 a.u. The stress tensor of the MD runs at 80 Ry plane-wave cutoff was unconverged with respect to the basis set and therefore required correction. We calculated this correction term from single configurations and a converged plane-wave cutoff of 140 Ry. The difference in stress tensor was added as correction to the pressure of the MD run.[73]

We performed several simulation runs, modeling different degrees of polymerization (Table I). Each run was 50 ps of simulated time, and comprised the silica species plus 25-27 explicitly treated water molecules with periodic boundary conditions (except run POLY, with nominally 16 H_2O and 16 SiO_2 in a metastable single-phase state). Excluding the gas-phase runs, the total number of atoms in each of the bulk runs was between 90 and 100. The temperature was 300 K or 1000 K, and it was controlled by Nosé-Hoover-chains for each degree of freedom ("massive" thermostating[74]). The runs were carried out in the NVT (canonical) ensemble, where volume and temperature were kept constant. The density was adjusted such that the average pressure at 1000 K would be close to 0.5 GPa. For a discussion of the validity of the mode-projection approach at extreme temperatures see Section II B 5.

B. Decomposition of the vibrational spectrum

Experimental vibrational spectra of silica species in solution, in a glass or in a melt in the frequency range between about 400 cm^{-1} and 1200 cm^{-1} contain contributions from quasi-local vibrational modes that reflect the local environment. These contributions are commonly evaluated (e.g. in Raman spectroscopy) in terms of the degree of polymerization. They arise from quasi-normal-modes of mainly two natural structural subunits of the silicate network, the SiO_4 tetrahedron and the Si-O-Si bridging oxygen (BO) (Fig. 1). Through all stages of polymerization (i.e., all possible Q^n species of a tetrahedron), the character of their vibrational motions remains the same (normal-mode-like), but the frequencies shift.

In the computational analysis of MD trajectories, the spectral density (i.e., the power spectrum) of a group of atoms is calculated from the Fourier transform of their velocity autocorrelation function (VACF)

$$F(\omega) = \int_0^{t_{max}} cos(\omega t) dt \langle v_k(t) \cdot v_k(0) \rangle, \qquad (1)$$

where $F(\omega)$ is the spectral density and ω is the angular frequency, and chevrons indicate the ensemble average.[75] The details of equation 1 in this contribution are $t_{max} = 1$ ps (which yields a good compromise between usage of data and sharpness of the resulting spectrum), normalisation of the VACF to unity at $t = 0$ prior to Fourier transformation and a von-Hann-window function to reduce edge effects. Finally, the spectral density $F(\omega)$ is squared and smoothed via convolution with a Gaussian of $\sigma = 20\,cm^{-1}$ to facilitate the extraction of a single peak frequency.

If the complete, unprojected particle velocity vectors are used in equation 1, then the resulting spectral density is the complete vibrational density of states (VDOS), including translational, rotational and low-frequency long-range acoustic-like contributions (full VDOS, Fig. 3).

The mode-projection approach allows us to separate out each normal-mode-like quasi-local contribution of small, specific groups of atoms from the complete vibrational density. For this, the atomic velocity vectors are decomposed into different components before equation 1 is applied. In a first step, the atoms are grouped together according to the structural subunit of interest. In a second step, if the group consists of more than two particles, the translational movement of the group needs to be subtracted from the individual particle velocities, in order to remove non-local, low-frequency motions. This can be done by subtraction of the velocity of the center atom (the silicon in the case of the tetrahedron). Alternatively, the velocity of the center-of-mass of the group can be used. The center atom is used for subtraction throughout this study (for discussion of this choice see Section II B 5). In a third step after subtraction of the center velocity, the particle velocities are further decomposed by projection of atomic motions onto a set quasi-normal modes (QNMs) based strictly on symmetry.[48,51] We follow the methods described by Pavlatou *et al.*[51] and Taraskin and Elliott[48] in decomposing the VACF of silicon-bonded oxygen atoms by projecting the vibrations onto sets of vectors representing molecular normal modes of different molecular subunits. These QNMs approximate molecular normal modes, but may differ slightly from the true normal modes in that the particle velocities are relative to the center atom.

Four main symmetries of quasi-normal-mode (QNM) decomposition are used here: 1) The SiO_4 tetrahedron with symmetry T_d, 2) O-Si-O and Si-O-Si subunit vibrations into C_{2v} (H_2O-like) QNMs, 3) the ethane-like decomposition for the case of the $H_6Si_2O_7$ dimer and 4) the individual Si-OH stretching. See Figure 1 and Table II for combinations of

TABLE I: Overview of the simulation runs. The calculated pressure is about 0.5 GPa for all bulk cells.

run label	composition and species	temperature (K)	density (g/cm^3)
Monomers:			
MON-300K	H_4SiO_4 + 27 H_2O	300	0.95
MON-1000K	H_4SiO_4 + 27 H_2O	1000	0.95
Dimers:			
DIM-1000K	$H_6Si_2O_7$ + 25 H_2O	1000	1.02
DIM-GASMD-300K	$H_6Si_2O_7$	300	–
Linear trimer:			
TRIM	$H_8Si_3O_{10}$ + 23 H_2O	1000	1.09
Higher polymers:			
POLY	16 H_2O + 16 SiO_2 nominally	1000	1.88

modes and geometries.

1. SiO_4 tetrahedral (T_d) QNMs

A tetrahedral molecule has four normal modes which are in principle all Raman active and most of which are degenerate: ν_1^{TET} (symmetric stretch, A_1), ν_3^{TET} (asymmetric stretch, F_2), ν_2^{TET} (E-bending or symmetric bending, E) and ν_4^{TET} (umbrella-bending or asymmetric bending, F_2). A sketch of the derived quasi-normal modes (QNMs) is given in Fig. 1, top row. The individual instantaneous velocity vectors of all four oxygen atoms of a tetrahedron i can be projected onto the ν_1^{TET} symmetric stretch QNM by

$$V^i_{\nu_1^{TET}} = \sum_{j=1}^{4} v^{||}_{i,j}, \tag{2}$$

where $v^{||}_{ji}$ is the magnitude of the velocity of oxygen atom j projected onto the normalized displacement vector from oxygen atom j to the silicon of tetrahedron i. Analogously, the first degenerate component of the ν_3^{TET} asymmetric stretch normal mode is described by

$$V^{i,I}_{\nu_3^{TET}} = v^{||}_{i,1} + v^{||}_{i,2} - v^{||}_{i,3} - v^{||}_{i,4}. \tag{3}$$

The other two degenerate modes II and III are obtained by exchanging oxygen atom 2 with oxygens 3 and 4, respectively. Other combination do not yield linearly independent modes. In the present study, the degenerate components are logged individually and averaged only after Fourier transform.

One component of the ν_2^{TET} E-bending is obtained from projection

$$\begin{aligned} V^{i,I}_{\nu_2^{TET}} = &(v^{\perp}_{i,1} - v^{\perp}_{i,2}) \cdot (\hat{r}_{i,1} - \hat{r}_{i,2}) \\ &+ (v^{\perp}_{i,3} - v^{\perp}_{i,4}) \cdot (\hat{r}_{i,3} - \hat{r}_{i,4}). \end{aligned} \tag{4}$$

where $v^{\perp}_{i,j}$ is the vector component of the velocity of oxygen atom j of tetrahedron i, perpendicular to Si-O, and $\hat{r}_{i,j}$ is the displacement vector from oxygen atom j to the silicon of tetrahedron i. The second component is obtained by interchanging the velocity and displacement vectors of oxygen atom 2 with those of oxygen atom 3.

One component of the ν_4^{TET} umbrella-bending can be computed from

$$V^{i,I}_{\nu_4^{TET}} = (v^{||}_{i,2} - v^{||}_{i,3} - v^{||}_{i,4}) \cdot \hat{r}_{i,1}. \tag{5}$$

The other two components can be obtained by interchanging the velocity and displacement vectors of oxygen atom 1 those of oxygen atom 2 and 3, respectively.

2. Bridging oxygen QNMs (C_{2v})

There are three structural subunits of silica with C_{2v} symmetry: 1) the Si-O-Si bridging oxygen (BO) atoms, 2) the non-bridging oxygen O-Si-O (HO-Si-OH) and 3) the bridging oxygen O-Si-O (Si-O-Si-O-Si). The first is designated by the superscript "BO", the latter two are designated by the superscript "OSiO". Here, we derive the QNM projections for the BO, and the OSiO QNMs are analogous. The C_{2v} normal modes are ν_1^{BO} symmetric stretch (A_1), ν_3^{BO} asymmetric stretch (B_2) and ν_2^{BO} bending (A_1) (Fig. 1, for normal modes see e.g. McMillan and Hofmeister[77] and Taraskin and Elliott[48]).

The ν_1^{BO} symmetric stretch is, analogous to the tetrahedral case, the sum of Si-O parallel projections as

$$V^i_{\nu_1^{BO}} = v^{||}_{i,1} + v^{||}_{i,2}, \tag{6}$$

the ν_3^{BO} asymmetric stretch is

$$V^i_{\nu_3^{BO}} = v^{||}_{i,1} - v^{||}_{i,2}, \tag{7}$$

and the ν_2^{BO} bending is

$$V^i_{\nu_2^{BO}} = (v^{\perp}_{i,1} - v^{\perp}_{i,2}) \cdot (\hat{r}_{i,1} - \hat{r}_{i,2}). \tag{8}$$

Another way of decomposing the bridging-oxygen atom motions are the three orthogonal directions $v_{BO} = v_B + v_R + v_S$, related to bending, rocking and stretching (B-R-S) motions.[48]

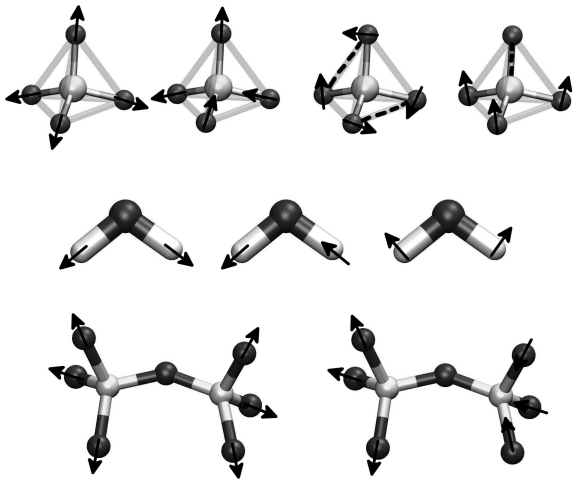

FIG. 1: Three sets of quasi-normal modes (QNMs) considered in this study. Top row: QNMs of a tetrahedral molecule of symmetry T_d. From left to right: ν_1^{TET} (symmetric stretch), ν_3^{TET} (asymmetric stretch), ν_2^{TET} (symmetric bending, here and elsewhere referred to as E-bending) and ν_4^{TET} (asymmetric bending, here and elsewhere referred to as umbrella-bending). Arrows indicate the velocity component of interest. Dashed lines in bending modes represent additional projection vectors where a second projection is necessary. Middle row: The C_{2v} QNMs for bridging oxygen Si-O-Si and geminal oxygen O-Si-O parts of Q^2-species. From left to right: ν_1^{BO} symmetric stretch, ν_3^{BO} asymmetric stretch and ν_2^{BO} bending. Bottom row: Two ethane-like QNMs of the Si_2O_7 dimer: ν_1^{DIM} symmetric stretch and ν_3^{DIM} asymmetric stretch. The structures were drawn using the *VMD* software package[76].

However, there are redundancies between the C_{2v} and the B-R-S concepts, only the low-frequency rocking contribution is not captured by the C_{2v} BO concept. Therefore we focus on the C_{2v} results. More vibrations of H_2O-like structural sub-units are possible, like NBO-Si-NBO wagging, scissoring and twisting. However, these vibrations cannot cannot be derived from C_{2v} (H_2O-like) normal modes and do not play a role in silicates. It is not considered here and mentioned only for completeness.

3. $H_6Si_2O_7$ dimer ethane-like QNMs

The $H_6Si_2O_7$ dimer shows vibrational motions that cannot be reduced to Q^1 tetrahedral motions alone.[24,57] There is coupling of stretching vibrations across the two tetrahedra, which is similar to two normal modes of the C_2H_6 ethane molecule. Therefore, the ethane-like ν_1^{DIM} symmetric stretch QNM is computed from the contributions of the six non-bridging oxygen atoms (see Fig. 1)

$$V^{1+2}_{\nu_1^{DIM}} = \sum_{j=1}^{3} v^{||}_{1,j} + \sum_{j=1}^{3} v^{||}_{2,j}, \tag{9}$$

and the ν_3^{DIM} asymmetric stretch is

$$V^{1+2}_{\nu_3^{DIM}} = \sum_{j=1}^{3} v^{||}_{1,j} - \sum_{j=1}^{3} v^{||}_{2,j}. \tag{10}$$

4. The individual Si-OH stretching

The Si-OH stretching of hydrogen-terminated, non-bridging oxygen atoms is recorded as the projection of instantaneous oxygen velocity onto the Si-O translation vector. It will be evaluated separately for Q^0- to Q^3-species. The hydrogen atoms are not considered explicitly, as is discussed in the following Subsection.

5. The validity of the silica mode-projection approach

The mode-projection approach and the above described projection sets exploit the fact that the high-frequency vibrations of the silica species in any degree of polymerization are normal-mode-like and quasi-localized. The mode-projection approach requires the choice of a center of a structure of interest for two reasons. Firstly, the translational motion of the structure as a whole needs to subtracted, as described above. Secondly, a center is needed for the construction of the displacement vectors that form the projection basis. The choice of the silicon atom as reference center of the QNM is justified because the velocity of each oxygen atom represents part of a vibration of the Si-O bond. An alternative choice, the center-of-mass of the tetrahedron, can also be used as the center of the projection. The resulting spectral density distribution is very similar (see Fig. 2) and the spectral density peak frequencies are almost identical. This similarity of results from different sets of projection vectors implicitly demonstrates that the tetrahedral distortion at high temperatures does not significantly affect the resulting peak frequencies. The projection on the displacement vectors of an undistorted, ideal tetrahedron would not give different results. Throughout this contribution, we use the silicon atom as reference center of the QNMs.

The QNMs are not strictly speaking orthogonal to each other. Their projections overlap. In the case of the tetrahedral QNMs, this is a result from the fact that the motion of the silicon in its oxygen cage is neglected in the QNMs (Fig. 3). In the case of ν_1^{BO} and ν_1^{DIM}, this results from the similarity of the atomic motions. As a consequence, the QNM projection does not exclude that some normal-mode-like motions are recorded not only by one QNM, but in a weaker degree also by a second one. In other words, the definition of our QNM projections leads to a geometrically not completely decoupled recording of atomic velocity components. This produces (artificial and usually weak) "ghost" spectral density, as

in the v_3^{TET} and v_4^{TET} in Fig. 2. The exchange of the reference center from the silicon atom to the center-of-mass flips the "ghost" spectral density from v_3^{TET} to v_4^{TET}. This shows that the reason for this artifact is the neglect of the motion of the silicon atom, whose own "cage rattling" spectral density is shown in grey. This transfer of spectral densities does not cause complications in the interpretation of subspectra. We point to this effect wherever it occurs.

In this study, we restrict ourselves to the analysis of the vibrations of the oxygen and silicon atoms. The motions of the hydrogen atoms are not explicitly considered. This is justified as follows. It is well known that the spectroscopically important frequency range of 400-1100 cm^{-1} is dominated by the Si-O stretching and bending motions of different silica species. O-H stretching motions occur at $>3000\,cm^{-1}$ (e.g., Zotov and Keppler[15]). SiOH bending motions occur at about $1200\,cm^{-1}$.[78,79] As structural environment, the hydrogen atoms affect the frequency of Si-O vibrations implicitly. Because of low mass, the hydrogen atomic positions and their velocities do not have to be included explicitly in the analysis of the quasi-normal modes of silica structural subunits. All the effects of bonded hydrogen on the Si-O vibrations of the tetrahedral units are implicitly included in our calculations because they are included in the MD simulations. Our procedure is only very weakly sensitive to variations in the representation of the hydrogen bonding caused by different exchange-correlation functionals. At 1000 K and below, as in the present study, no Si-O bonds are broken on the timescale of our MD runs. Only occasionally, a hydrogen atoms of a hydroxy site is exchanged with one of the surrounding water molecules. This has no measureable effect on the spectral density of any QNM.

The high vibrational bandwidths in all Figures result from a combination of two effects. Firstly, the structure is disordered. This creates a bandwidth due to the damping of vibrational modes. Also, it causes a variation of the exact structural environment between every individual tetrahedron. At the stage of averaging the results for every Q^n species, this introduces band broadening. Secondly and mainly, the high width at half maximum of about $200\,cm^{-1}$ is an artifact resulting from limited ensemble averaging. Longer MD runs or larger cells would produce sharper subspectra, however, it is computationally too demanding.

Based on the comparison of power spectra from different time segments of a MD trajectory, the error of the present peak frequencies is estimated to be between $10\,cm^{-1}$ and $30\,cm^{-1}$, depending on 1) the degree of spread of the power spectrum of a specific quasi-normal mode and 2) on the character of the vibrational motion. High-frequency, "stiff" tetrahedral stretching vibrations have a smaller error. The Si-O-Si modes have a larger error due to the additional structural degree of freedom of the Si-O-Si bending angle which significantly affects all vibrational frequencies of the bridging oxygen (see e.g. Hunt *et al.*[16]).

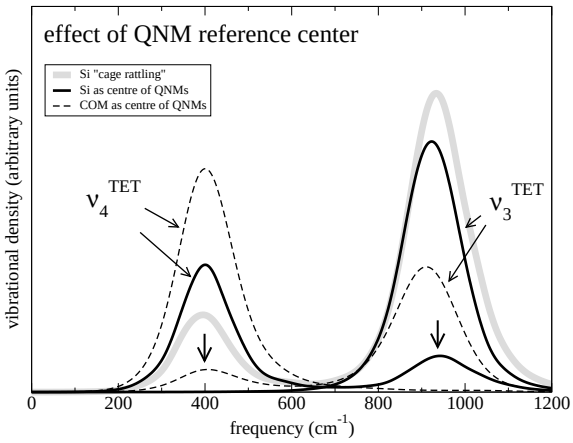

FIG. 2: For v_3^{TET} and v_4^{TET}, the difference in spectral density is demonstrated caused by using either the silicon atom or the tetrahedral center-of-mass (COM) as projection reference center. Silicon as reference center introduces an artifical high-frequency contribution to v_4^{TET} (right arrow) as discussed in Section II B 5. The center-of-mass as reference center causes an artificial low-frequency contribution to v_3^{TET} (left arrow). This frequency overlap results from the silicon atom "cage rattling" motions (grey). Throughout this study the silicon is used as reference center. Spectra are scaled by 1.039.

III. RESULTS

There is a large amount of information resulting from the application of the different sets of QNMs to the different structural subunits. We restrict ourselves to a few stretching modes that appear to us of greatest importance for Raman spectra of dissolved silica and we give particular emphasis to those modes that are subject to some ambiguity in terms of band assignment. We present frequencies of peaks in spectral density, focusing on five major findings: 1) the neutral monomer as a benchmark of the technique, 2) the evolution of the tetrahedral stretches with increasing degree of polymerization and the special case of Q^2-species, 3) the single Si-OH stretching on tetrahedra of increasing degree of polymerization and the origin of the Raman band at $970\,cm^{-1}$ in hydrous silica, 4) the evolution of the BO stretching modes with increasing polymerization and 5) the dimer with two unique modes.

In this Section, all depicted spectra and extracted frequencies are scaled by 1.039 to account for the systematic error of the ab initio method used here. In Section IV A the derivation of this scaling factor is discussed. We evaluate the spectral densities in terms of their peak frequencies. In Table III both scaled and unscaled spectral density peak frequencies of stretching QNMs are listed.

TABLE II: Quasi-normal modes (QNMs) discussed in this study. Other QNMs were also derived, but are not considered further because they are less relevant to Raman band assigments in experimental studies.

Mode:	applied to:	abbreviation:	in Figure:
single oxygen mode:			
single Si-O stretch	any oxygen atom	–	7
tetrahedral QNMs (T_d):			
symmetric stretch (A_1)	any Q^n-species	ν_1^{TET}	3,4,6
asymmetric stretch (F_2)	any Q^n-species	ν_3^{TET}	3,5
E-bending (E)	any Q^n-species	ν_2^{TET}	3
umbrella-bending (F_2)	any Q^n-species	ν_4^{TET}	3
BO QNMs (H_2O-like, C_{2v}):			
Si-O-Si symmetric stretch (A_1)	any bridging oxygen	ν_1^{BO}	8
Si-O-Si asymmetric stretch (B_2)	any bridging oxygen	ν_3^{BO}	9
Si-O-Si bending (A_1)	any bridging oxygen	ν_2^{BO}	–
Q^2 BO and NBO (C_{2v}):			
O-Si-O symmetric stretch (A_1)	Q^2 BO/NBO pair	ν_1^{OSiO}	6
O-Si-O asymmetric stretch (B_2)	Q^2 BO/NBO pair	ν_3^{OSiO}	6
O-Si-O bending (A_1)	Q^2 BO/NBO pair	ν_2^{OSiO}	–
ethane-like QNMs:			
symmetric stretch (A_1)	dimer	ν_1^{DIM}	10
asymmetric stretch (B_2)	dimer	ν_3^{DIM}	10

A. The tetrahedral QNMs of the H_4SiO_4 monomer

The H_4SiO_4 monomer is a test case for the mode-projection approach, because a several computational studies have calculated the NMA frequencies to which our results can be compared (see Section I). In Fig. 3, the spectral densities of the four tetrahedral QNMs of the H_4SiO_4 monomer are shown for 300 K and 1000 K. All QNMs show a weak decreasing trend in frequency upon increasing temperature, as is expected from theory and experiment (see e.g. Zotov and Keppler[15]). The ν_1^{TET} is at 774 cm^{-1} for 300 K and at 762 cm^{-1} for 1000 K. These frequencies match experimental ones very closely because both frequencies were used for the derivation of the scaling factor of 1.039 (Section IV A). At 1000 K, ν_3^{TET} is at 920 cm^{-1}, ν_2^{TET} at 291 cm^{-1} and ν_4^{TET} at 405 cm^{-1}. The weak high-frequency peak of ν_4^{TET} at about 935 cm^{-1} is an artifical contribution as discussed in Section II B 5. Also in Fig. 3, we plot literature data for comparison. These explicitly calculated frequencies from NMA represent very Raman intense normal modes of the monomer.

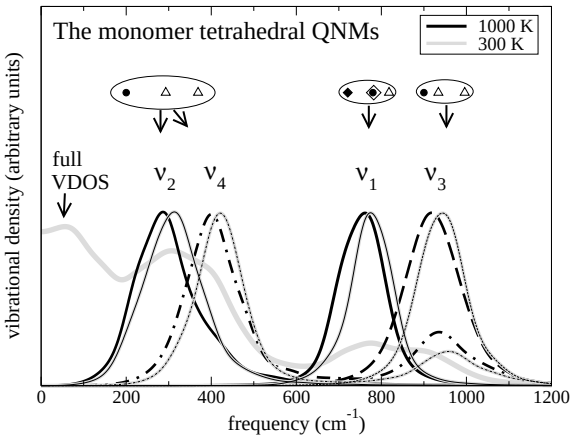

FIG. 3: Spectral density of the four tetrahedral QNMs of the silicate monomer (1000 K and 300 K). For QNM abbreviations see Table II. The full VDOS is plotted for comparison. All spectral densities are scaled by 1.039 (see Section IV A). Symbols represent literature data of monomer vibrational frequencies with Raman activity higher than 1% of that of the ν_1^{TET} symmetric stretch near 770 cm^{-1}. Empty diamond: Zotov and Keppler[15] (bond polarizability model). Filled diamond: Tossell[57] (MP2). Circles: Lasaga and Gibbs[24] (Hartree-Fock). Triangles: DeAlmeida and OḾalley[25] (Hartree-Fock).

B. Tetrahedral symmetric stretching of higher Q^n-species

Higher-order silicate polymers exhibit a polymerization-driven systematic trend in the frequencies of most vibrational modes, which is reflected in the QNM results. This shift is especially important for the very Raman intense ν_1^{TET} mode. The spectral density peak frequency shifts from 761 cm^{-1} (Q^0) via 793 cm^{-1} (Q^1) and 1103 cm^{-1} (Q^3) to 1149 cm^{-1} (Q^4) (Fig. 4, inset in Fig. 5 and Table III). The broad contribution of the Q^2 ν_1^{TET} will be discussed below. All calculated spectra of Q^n-species shown in Fig. 4 are averaged over several tetrahedra of the same degree of polymerization, namely 2 tetrahedra for Q^0, 2 for Q^1, 6 each for Q^2 and Q^3, and 3 tetrahedra for Q^4. This improves the counting statistics of the peak shapes and positions.

The ν_3^{TET} also possesses a high Raman intensity in the case of the H_4SiO_4, as the literature data in Fig. 3 show. It also shows a polymerization-driven shift to higher frequencies. The ν_3^{TET} peak frequency of Q^0 is 920 cm^{-1}, for Q^1

942 cm^{-1}, for Q^2 970 cm^{-1}, for Q^3 1015 cm^{-1} and for Q^4 it is 1062 cm^{-1} (Fig. 5 and inset in Fig. 5). The latter value is in excellent agreement to the intense experimental band at 1060 cm^{-1} in pure dry silica glass which originates from the Q^4 ν_3^{TET}.[50] There is a frequency crossover of ν_1^{TET} and ν_3^{TET} with increasing polymerization (inset in Fig. 5). The ν_3^{TET} has a higher peak frequency than the ν_1^{TET} for low polymerized Q^0- and Q^1-species, but lower a lower peak frequency than the ν_1^{TET} for higher polymerized Q^3- and Q^4-species (Figs. 4 and 5). The Q^2 shows a double character.

The double character of Q^2 is reflected in its ν_1^{TET} double peak at 888 cm^{-1} and 1081 cm^{-1} (Fig. 6). The third ν_1^{TET} contribution at 701 cm^{-1} is an artifact of ν_1^{BO} as discussed in Section II B 5. All six Q^2-species used in the averaging show almost identical behavior. The two peaks of the Q^2 ν_1^{TET} can be explained by the motions of the smaller O-Si-O subunits (Fig. 6). The 888 cm^{-1} contribution arises from the ν_1^{OSiO} of the non-bridging NBO-Si-NBO, the 1081 cm^{-1} contribution stems from the analogous bridging oxygen BO-Si-BO ν_1^{OSiO}.

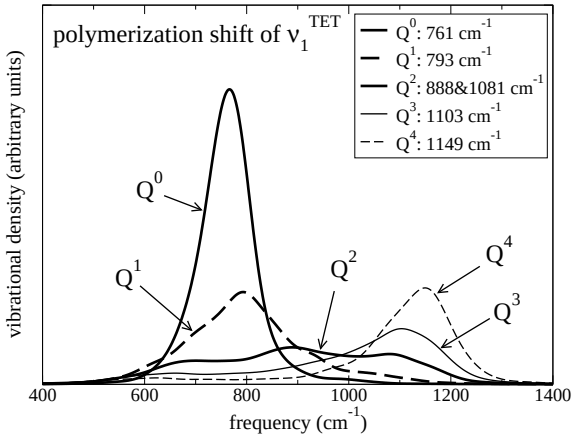

FIG. 4: The polymerization-driven ν_1^{TET} frequency shift from 762 cm^{-1} for Q^0-species to 1149 cm^{-1} for Q^4-species. Spectral densities are scaled by 1.039.

C. Single Si-OH stretching

The spectral densities of single non-bridging Si-OH stretching are shown for several Q^n-species in Fig. 7. Almost independent of the degree of polymerization of the respective tetrahedron, the peak frequency is between 915 cm^{-1} for Q^0-species and 925 cm^{-1} for Q^3-species (Table III). This finding is important for hydrous silica glasses, because commonly a band at 970 cm^{-1} has been assigned to Si-OH stretching.[18–20]

D. The bridging oxygen QNMs

The different degrees of polymerization of bridging oxygen (BO) atoms are described by the Q^n-Q^m notation which indicates the degree of polymerization of the adjacent two tetrahedra. The Q^n-Q^m-specific subspectra in Figures 8 and 9 are mostly averages over several BO atoms. The number of BO atoms used for every Q^n-Q^m combination are 1 for Q^1-Q^1, 2 for Q^1-Q^2, 7 for Q^2-Q^3, 5 for Q^2-Q^4, 3 for Q^3-Q^3, 5 for Q^3-Q^4 and 1 for Q^4-Q^4. The Si-O-Si ν_1^{BO} peak frequency in Fig. 8 is at about 620 cm^{-1} for the lowest possible degree of polymerization (i.e. Q^1-Q^1). For Q^1-Q^2 it is at about 680 cm^{-1}. For all higher polymerized bridging oxygens the peak frequency

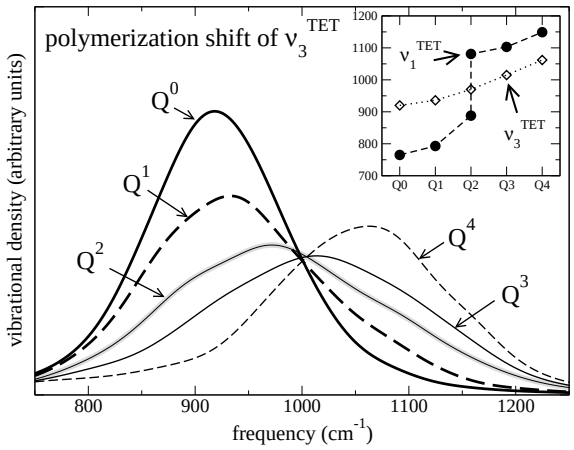

FIG. 5: The polymerization-driven frequency shift of the ν_3^{TET} asymmetric stretch from Q^0- to Q^4-species. Spectral densities are scaled by 1.039. Inset: The frequency shift of ν_1^{TET} and ν_3^{TET} with increasing Q^n-speciation. Note the cross-over of the ν_3^{TET} and ν_1^{TET} at Q^2-species.

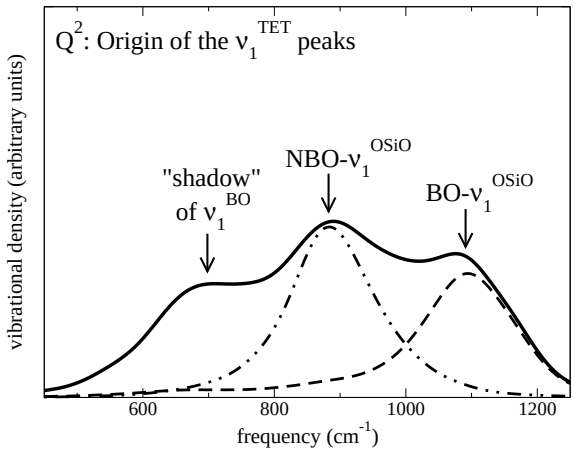

FIG. 6: The two high-frequency peaks of the Q^2 ν_1^{TET} originates from the vibrations of the O-Si-O units of the Q^2-species, namely the non-bridging NBO-Si-NBO ν_1^{OSiO} and the bridging oxygen BO-Si-BO ν_1^{OSiO}. The peak at 701 cm^{-1} is an artifact due to transmission of ν_1^{BO} vibrations into Q^2 ν_1^{TET}, as discussed in Section II B 5. All spectra are scaled by 1.039.

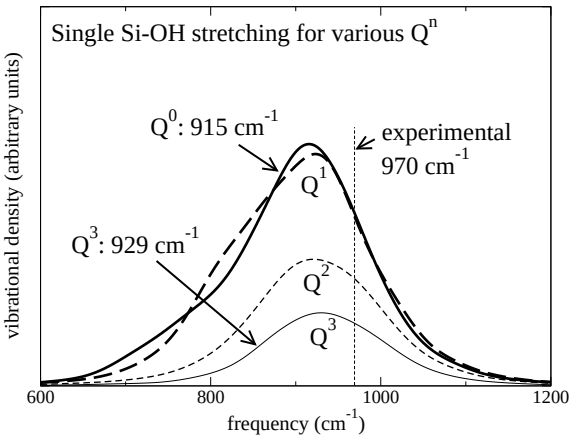

FIG. 7: The single non-bridging oxygen Si-OH stretching for different degrees of polymerization of the tetrahedron. Spectra are scaled by 1.039.

is around 780 cm^{-1}. The second peak in the spectral density of Q^1-Q^1 at 880 cm^{-1} (and to a lesser extent, for Q^1-Q^2) is an artifact as discussed in Section II B 5. The Si-O-Si ν_3^{BO} is centered between 1050 cm^{-1} and 1060 cm^{-1}, with only a slight trend towards higher frequencies upon increasing polymerization (Fig. 9). This study focuses on the high-frequency silica stretching modes, therefore we do not consider the ν_2^{BO} bending here.

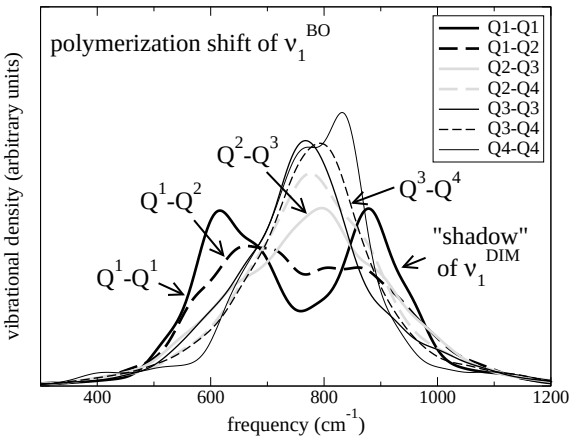

FIG. 8: The bridging oxygen ν_1^{BO} for various degrees of polymerization. All spectra are scaled by 1.039. Note the frequency shift with increasing polymerization from 620 cm^{-1} for Q^1-Q^1 to about 780 cm^{-1} for Q^1-Q^1 and even higher degrees of polymerization.

E. The $H_6Si_2O_7$ dimer QNMs

Two runs have been carried out for the dimer, changing temperature and bulk/gas-phase (Table I). The ν_1^{TET} of the two individual Q^1 tetrahedra is at 793 cm^{-1}, as has been discussed in Section III B. The ethane-like ν_1^{DIM} shows a relatively narrow peak at about 870 cm^{-1} (Fig. 10). The same mode in the gas-phase run at 300 K was observed at 845 cm^{-1} (Table III). The peak of the ν_3^{DIM} is at 783 cm^{-1} at 1000 K and at 785 cm^{-1} at 300 K. Counter-intuitively, the ν_1^{DIM} is higher in frequency than the ν_3^{DIM}.

FIG. 9: The bridging oxygen ν_3^{BO} for various degrees of polymerization. All spectra are scaled by 1.039.

FIG. 10: The dimer ethane-like ν_1^{DIM} and ν_3^{DIM}, and two tetrahedral QNMs for comparison. Spectra are scaled by 1.039.

IV. DISCUSSION

A. Benchmarking and scaling: The H_4SiO_4 monomer

The ν_1^{TET} is by far the most Raman-intense mode of the silicic-acid monomer and its assignment is well established (Fig. 11 and citations in Section I). Therefore, we use this mode for the derivation of a scaling factor to account for

TABLE III: Overview over the frequency results of tetrahedral and dimer stretching QNMs. The two monomer symmetric stretch results have been used to derive an averaged scaling factor (SF) of 1.039. For mode abbreviations see Table II. The uncertainty is estimated to be about 10 to 30 cm^{-1} (see Section II B 5)

species, mode and run:	see Figure:	unscaled freq.: (cm^{-1})	scaled freq.: (cm^{-1})	annotations:
ν_1^{TET}:				
Q^0, from MON-1000K	3	733	765 (SF 1.044)	Exp: 765[2]; SF derived here: 1.044
Q^0, from MON-300K		745	770 (SF 1.033)	Exp: 770[2]; SF derived here: 1.033
Q^1, from DIM-1000K and TRIM	4,10	763	793	close to Q^0 ν_1^{TET}
Q^2, from POLY (av of 6)	6	855+1040	888+1081	two peaks. Third at 700 is an artifact
Q^3, from POLY (av of 3)	4	1062	1103	good agreement with literature[4,26]
Q^4, from run POLY (1 only)	4	1106	1149	good agreement with literature[4,26]
ν_3^{TET}:				
Q^0, from MON-1000K	3	885	920	
Q^0, from MON-300K	3	907	942	
Q^1, from DIM-1000K and TRIM	5,10	901	936	
Q^2, from POLY (av of 6)	5	934	970	
Q^3, from POLY (av of 6)	5	977	1015	
Q^4, from POLY (av of 3)	5	1023	1062	
single NBO Si-OH stretch:				
Q^0 (Q^3)	7	881 (894)	915 (929)	almost no shift with incr. polym.
Dimer QNMs:				
ν_1^{DIM}, from DIM-1000K (DIM-GASMD-300K)	10	837 (813)	870 (845)	good agreement with literature[57]
ν_3^{DIM}, from DIM-1000K (DIM-GASMD-300K)	10	754 (756)	783 (785)	

the systematic error of the ab initio calculations used here and to align the calculated frequencies with the values measured in experiment.[57] The frequency agreement of our results of about 745 cm^{-1} (300 K) and 733 cm^{-1} (1000 K) to published NMA results[15,24,25,31–33,57,78] is good (Fig. 3 and Table III). The experimental frequency of the ν_1^{TET} occurs at about 775 ± 10 cm^{-1}.[80] It is weakly temperature dependent: 770 cm^{-1} at 300 K and 765 cm^{-1} at 1000 K.[15] From these two experimental frequencies and the results of the monomer MD runs, the frequency ratios give scaling factors of 1.044 and 1.033 for 300 K and 1000 K (Table III). These factors are in good agreement to common frequency scaling factors.[57] We used the averaged scaling factor of 1.039 throughout this study.

For benchmarking, Figure 3 shows computed frequencies of modes with high Raman activity from the gas-phase cluster modeling literature.[15,24,25] These modes have a Raman intensity of at least 1% of that of the most intense mode. These results were calculated using various reliable techniques up to Hartree-Fock level. The scatter between these results represents differences produced by different theoretical approaches (Hartree-Fock, MP2 and classical potential; Fig. 3). The spectral densities of the four tetrahedral QNMs used here covers the Raman scattering vibrations of the complete H_4SiO_4 monomer in the spectral region of interest up to 1200 cm^{-1} (Fig. 3). This gives us confidence in the mode-projected VACF approach: The application of tetrahedral QNMs to the H_4SiO_4 monomer produces spectral density peaks in all the frequency regions where there are known Raman-spectroscopically important modes of the H_4SiO_4 monomer (Fig. 3).

B. Comparison to experimental results

Because the aim of our study is to assist band assignment, we show our results in comparison to the work of Zotov and Keppler[15] and Mysen and Virgo[81] (Fig. 11). The most important QNM peak frequency results are indicated. These are likely the most Raman intense modes in the frequency range between 600 cm^{-1} and 1200 cm^{-1}, but we do not claim completeness. However, our findings have the potential to explain important features of Raman spectra of the system SiO_2-H_2O.

C. Behavior of ν_1^{TET} and ν_3^{TET} with increasing polymerization

The ν_1^{TET} is a strong Raman scatterer in silica species. From all possible Q^n-species together, it is probably responsible for the largest part of Raman intensity between 770 cm^{-1} and 1150 cm^{-1} (see e.g. McMillan[1], also Fig. 11). Its vibrational contribution remains localized in frequency range during increasing polymerization (Fig. 4). The Q^0 ν_1^{TET} has been used by us to derive the scaling factor of 1.039 (Section IV A, Table III). The Q^1 ν_1^{TET} is at 793 cm^{-1}. This is very close to the frequency of Q^0. Experimental studies assign a band centered at 850 cm^{-1} (Fig. 11) to Q^1-species (Mysen[4], for similar assignment in potassium silicate melt see Malfait *et al.*[26]). This apparent contradiction is resolved below (Section IV F). However, the Q^1 ν_1^{TET} at about 793 cm^{-1} points to an asymmetry of the Q^0 770 cm^{-1} band which can be observed in Figure 11 (see also Dutta and Shieh[10] and Zotov and Keppler[15]). Q^3- and Q^4-species have been assigned to Raman intensity between 1100 cm^{-1} to 1150 cm^{-1} in silica glass or sodium silicate glasses.[1,4,5,26,82] Our results of 1103 cm^{-1} for Q^3 and

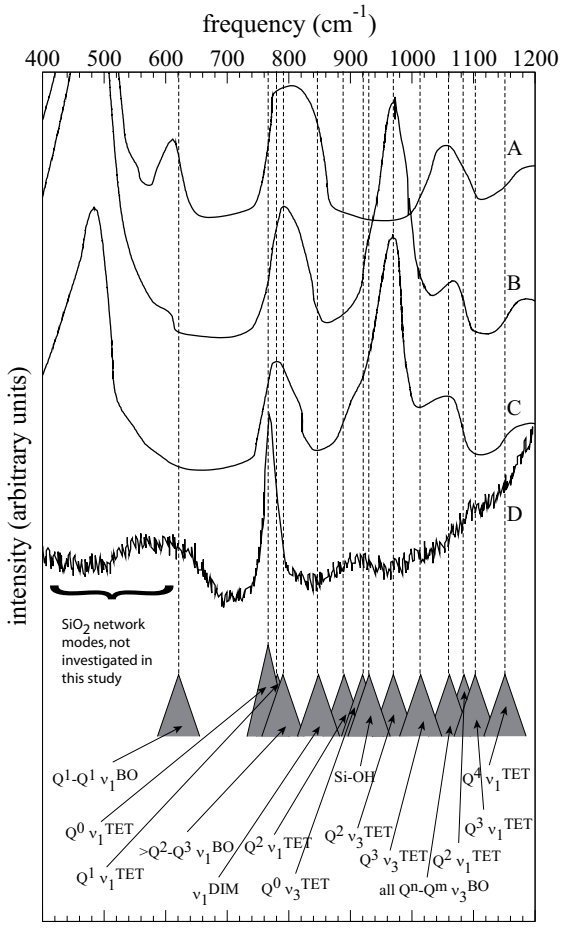

FIG. 11: Upper part: Four experimental Raman spectra of the system SiO_2-H_2O. Lower part: Selected species- and mode-specific frequencies determined in the present study, scaled by 1.039. Spectrum (A): pure SiO_2 glass.[81] Spectrum (B) and (C): SiO_2 with 10wt% H_2O and 5wt% H_2O, respectively.[81] Spectrum (D): Silica in aqueous solution at 900 ∘C and 1.4 GPa.[15] Note that the intensity shoulder from about 1000 cm^{-1} is due to the diamond anvil cell.

1149 cm^{-1} for Q^4 are in good agreement with these assignments. The frequency difference between the high-frequency peak of Q^2 at 1081 cm^{-1} and the Q^3 at 1103 cm^{-1} is quite small, which will make their distinction in experiment difficult, unless the lower-frequency peak of Q^2 at 888 cm^{-1} is also taken into consideration (Table III). In Figure 11, the extension of the high-frequency shoulder to 1100 cm^{-1} and beyond with increasing silica content can be explained by an increase in Q^2-species.

The spectral density of the ν_1^{TET} of polymerized tetrahedra is narrowest when oxygen atoms of the Q^n-species are either all non-bridging (Q^0) or when they are all bridging (Q^4), but wider for intermediate Q^n-species. The Q^2-species show the broadest spectral density (Fig. 4), with two distinct peaks (Fig. 6). This double peak and its intermediate character between low and high degree of polymerization (inset in Fig. 5) may be the reason for the still debated assignment of peaks to Q^2-species.[4,26] In Raman spectra of a potassium silicate melt, Malfait *et al.*[26] assigned two peaks at 920 cm^{-1} and 1070 cm^{-1} to Q^2-species, based on correlated intensities. Our two peaks at 888 cm^{-1} and 1081 cm^{-1} are in good agreement with this. These results 1) give further evidence for the observation that Q^2-species produce a double peak[26,40], and 2) show that the two experimentally found Q^2 band are probably caused by a double peak of the ν_1^{TET}.

Our result of the ν_3^{TET} of Q^0-species at 920 cm^{-1} is in close agreement to an experimental band at 925 cm^{-1} in the lowest silica concentration (Fig. 11). The relative significance of this band decreases with increasing silica concentration. However, this may be a result of increasing Raman intensity around that band rather than a real decrease of the 925 cm^{-1} band (Fig. 11). A direct tracing of the ν_3^{TET} with increasing degree of polymerization is not possible in the experimental spectra, because it is too weak.

D. Single non-bridging oxygen Si-OH stretching and the origin of the 970 cm^{-1} band in hydrous silica

In hydrous silica glass, there is a band at 970 cm^{-1}, which is usually interpreted as arising from a defect structure and commonly assigned to Si-OH stretching of Q^3-species.[18–20] A weak band at 910-915 cm^{-1} is also present[18–20], that has been assigned only once, to an SiOH vibration of two geminal silanol groups (i.e., to Q^2-species).[19] Our results show that the individual SiOH stretching is at about 930 cm^{-1} for Q^3 and at about 920 cm^{-1} for Q^2 (Table III). This suggests that the individual SiOH stretching vibrations may not be the reason for the band at 970 cm^{-1}. Also, the Q^3 ν_1^{TET} at about 1100 cm^{-1} and ν_3^{TET} at about 1015 cm^{-1} are not near the 970 cm^{-1} band. Therefore, we suggest that they are also less likely the reason for this band. NMR is a sensitive probe for Q^n-species in silica glass.[23,30,83] It has been shown by a recent NMR study that, besides Q^3-species, also a significant amount of Q^2-species can be present in hydrous silica glass.[23] We observe the ν_3^{TET} of Q^2-species at 970 cm^{-1} (Table III). However, the origin of the 970 cm^{-1} band cannot be decided on the basis of this point, and further investigation is needed.

E. The BO stretching vibrations

The ν_1^{BO} is strongly dependent on the degree of polymerization of the two adjacent tetrahedra (Fig. 8). The weakest state of polymerization of a BO is Q^1-Q^1, whose ν_1^{BO} shows a peak frequency at 620 cm^{-1}. The second peak of the Q^1-Q^1 at about 845 cm^{-1} is an artifact of the ν_1^{DIM} as discussed in Section II B 5. There is a polymerization-driven shift from 618 cm^{-1} to peaks between 780 cm^{-1} and 830 cm^{-1} (Fig. 9). These results agree with several experimental observations. Firstly, the experimental peaks around 600 cm^{-1} vanish with increasing polymerization. In pure SiO_2, there is only a peak in that frequency range resulting from small silica

rings.[1,38,39,84] Secondly, in several experimental studies the peak at about 630 cm^{-1} was interpreted as resulting from Si-O-Si vibrations of weakly polymerized species.[4,10,20] The Raman band around 800 cm^{-1} present in pure silica may rather be explained by the bridging oxygen asymmetric stretch than tetrahedral stretching.[84] Here again, the mode-projection technique gives a consistent picture of the evolution of frequencies with changing molecular structure.

The frequency of the peak center of ν_3^{BO} is at about 1070 cm^{-1} which is in good agreement to experimental observations.[4,5] It falls into the frequency region of the Q^3 and Q^4 ν_1^{TET}. Contrary to ν_1^{BO}, the ν_3^{BO} does not show significant shifts with higher degree of polymerization. The ν_3^{BO} has a high Raman intensity on the case of the $H_6Si_2O_7$ dimer. It is likely that this mode keeps an important Raman intensity with increasing degree of polymerization. The presence of this mode in the same frequency range of 1100 cm^{-1} to 1150 cm^{-1}, where most commonly only the Q^3- and Q^4-species are fitted, could have an important consequence: The degree of polymerization could be overestimated if all Raman intensity in this frequency region is explained by Q^3- and Q^4-species, but not by ν_3^{BO} as well.[85]

The ν_3^{BO} and the Q^4 ν_3^{TET} peak frequencies are both between 1060 cm^{-1} and 1070 cm^{-1} (Figs. 9 and 5). The ν_3^{BO} peak frequency is polymerization-independent, whereas the ν_3^{TET} shifts with increasing polymerization. It reaches the ν_3^{BO} peak frequency of about 1060 cm^{-1} in the case of Q^4-species, when every oxygen is a bridging oxygen. Therefore, the 1060 cm^{-1} band in pure silica, which has been assigned to ν_3^{TET}[50], can as well be assigned to ν_3^{BO}.

F. The $H_6Si_2O_7$ dimer

The Q^1-species in aqueous fluid have been assigned to an experimentally observed peak at 850 cm^{-1}.[1,4] Our results are in agreement with this assignment, and furthermore the calculations provide insight into which specific molecular vibrations are responsible for this band. The 850 cm^{-1} band does not appear to result from ν_1^{TET}. We observe the ν_1^{TET} of the Q^1 (Table III) at about 790 cm^{-1}, and the reproducibility across several simulations lends confidence to this value. The two Q^1 of a dimer do show an ethane-like coupling (ν_1^{DIM}, Table III) at about 870 cm^{-1} at 1000 K and at about 850 cm^{-1} in the gas-phase at 300 K. This is in good agreement with hybrid DFT calculations that predict very similar frequencies.[57] Thus, an experimentally observed peak at 850 cm^{-1} can be explained by the ethane-like ν_1^{DIM} mode of the dimer. A more detailed study on the vibrational properties of the dimer is in preparation.

V. CONCLUSIONS

In this study, new evidence is given to support common band assignments of silica in aqueous fluids and hydrous glasses: 1) Q^3 and Q^4 ν_1^{TET} have peaks around 1100 cm^{-1} and 1150 cm^{-1}, respectively; 2) the contribution of bridging oxygen ν_3^{BO} to bands with frequencies around 1070 cm^{-1}; and 3) the ν_1^{BO} in weakly polymerized species shows a peak around 600 cm^{-1}.

We find evidence for the assignment of several spectral features that have been hitherto ambiguous: 1) the Q^1 ν_1^{TET} shows a peak frequency of about 790 cm^{-1} which in experiments might be hidden by the strong 770 cm^{-1} band of the Q^0-species; 2) the Q^2 ν_1^{TET} exhibits a double-cusp band caused by its intermediate character between low and high degree of polymerization; 3) the dimer shows a peak between 870 cm^{-1} and 850 cm^{-1} resulting from the ethane-like ν_1^{DIM}, 3) the ν_1^{BO} shows a peak around 600 cm^{-1} only in the case of a degree of polymerization less than Q^2-Q^3, and 4) the 970 cm^{-1} band may possibly not result from individual Si-OH stretching (which we find at about 920 cm^{-1}).

The technique used here is comprehensive, i.e. any species can be considered, including charged species. It can be applied to other subsets of quasi-normal modes, e.g. octahedral ones, or larger structures such as silica rings. In doing so, it may provide insight into the origin of vibrational bands in pure silica glass, whose Raman spectrum is quite different from Raman spectra of polymerized silica species in solutions and glasses. Other, non-localized modes could be considered as well. The precision of this technique is only limited by the length of the molecular dynamics runs and the accuracy of the underlying framework of potential energy calculation. The species- and mode-selective subspectra presented here can be a reliable basis for the application of experimental analysis techniques like the principal component analysis.

ACKNOWLEDGMENTS

We thank two anonymous reviewers who helped to improve the manuscript. Our strategies for separating the contributions from local structural subunits benefited from conversations with Monika Koch-Müller. The calculations were partly performed on the BlueGene/P Jugene of the Jülich Supercomputing Centre (JSC) under project ID HPO15. GS and SJ acknowledge the financial support from the Deutsche Forschungsgemeinschaft (DFG) through the Grant No. JA1469/4-1 from the Emmy-Noether-Program. Support for MS-M was provided by the Institute for Critical Technology and Applied Science (ICTAS) at Virginia Tech, and by the National Science Foundation (NSF) under Grant No. OCE-0928472.

[1] P. McMillan, Structural studies of silicate glasses and melts: Applications and limitations of Raman spectroscopy, American Mineralogist 69 (1984) 622–644.

[2] N. Zotov, H. Keppler, Silica speciation in aqueous fluids at high pressures and high temperatures, Chemical Geology 184 (2002) 71–82.

[3] K. Mibe, I. M. Chou, W. A. Bassett, In situ Raman spectroscopic investigation of the structure of subduction-zone fluids, Journal of Geophysical Research 113 (2008) B04208.

[4] B. O. Mysen, Solution mechanisms of silicate in aqueous fluid and H_2O in coexisting silicate melts determined in situ at high pressure and high temperature, Geochimica et Cosmochimica Acta 73 (2009) 5748–5763.

[5] B. O. Mysen, Structure of H_2O-saturated peralkaline aluminosilicate melt and coexisting aluminosilicate-saturated aqueous fluid determined in situ to 800 °C and ∼800 MPa, Geochimica et Cosmochimica Acta 74 (2010) 4123–4139.

[6] D. Fortnum, J. O. Edwards, The Raman spectrum and the structure of the aqueous silicate ion, Journal of Inorganic and Nuclear Chemistry 2 (1956) 264–265.

[7] J. E. Earley, D. Fortnum, A. Wojcicki, J. O. Edwards, Constitution of aqueous oxyanions: Perrhenate, tellurate and silicate ions, Journal of the American Chemical Society 81 (1959) 1295–1301.

[8] R. Alvarez, D. L. Sparks, Polymerization of silicate anions in solutions at low concentrations, Nature 318 (1985) 649–651.

[9] P. Dutta, D. C. Shieh, Influence of alkali chlorides on distribution of aqueous base solubilized silicate species, Zeolites 5 (1985) 135–138.

[10] P. Dutta, D. C. Shieh, Raman spectral study of the composition of basic silicate solutions, Applied Spectroscopy 39 (1985) 343–346.

[11] M. Hosaka, S. Taki, Raman spectral studies of $SiO_2-NaOH-H_2O$ system solution under hydrothermal condtions, Journal of Crystal Growth 100 (1990) 343–346.

[12] R. Gout, G. S. Pokrovski, J. Schott, A. Zwick, Raman spectroscopic study of aluminum silicate complexation in acidic solutions from 25 to 150 °C, Journal of Solution Chemistry 28 (1) (1999) 73–82.

[13] R. Gout, G. S. Pokrovski, J. Schott, A. Zwick, Raman spectroscopic study of aluminum silicate complexes at 20 °C in basic solutions, Journal of Solution Chemistry 29 (12) (2000) 1173–1186.

[14] W. S. Bassett, A. H. Shen, M. Bucknum, I. M. Chou, A new diamond anvil cell for hydrothermal studies to 2.5 GPa and from -190 to 1200 °C, Review of Scientific Instruments 64 (1993) 2340–2345.

[15] N. Zotov, H. Keppler, In situ Raman spectra of dissolved silica species in aqueous fluids to 900 °C and 14 kbar, American Mineralogist 85 (2000) 600–604.

[16] J. D. Hunt, A. Kavner, E. A. Schauble, D. Snyder, C. E. Manning, Polymerization of aqueous silica in H_2O-K_2O solutions at 25-200 °C and 1 bar to 20 kbar, Chemical Geology 283 (2011) 161–170.

[17] S. C. Kohn, The dissolution mechanisms of water in silicate melts; a synthesis of recent data, Mineralogical Magazine 64 (3) (2000) 389–408.

[18] R. H. Stolen, G. E. Walrafen, Water and its relation to broken bond defects in fused silica, Journal of Chemical Physics 64 (6) (1976) 2623–2631.

[19] D. M. Krol, J. G. van Lierop, Raman study of the water adsorption on monolithic silica gels, Journal of Non-crystalline Solids 68 (1984) 163–166.

[20] P. F. McMillan, R. L. J. Remmele, Hydroxyl sites in SiO_2 glass: A note on infrared and Raman spectra, American Mineralogist 71 (1986) 772–778.

[21] P. F. McMillan, G. H. Wolf, B. T. Poe, Vibrational spectroscopy of silicate liquids and glasses, Chemical Geology 96 (1992) 351–366.

[22] H. W. Nesbitt, G. M. Bancroft, G. S. Henderson, R. Ho, K. N. Dalby, Y. Huang, Y. Z., Bridging, non-bridging and free (O^{2-}) oxygen in Na_2O-SiO_2 glasses: An x-ray photoelectron spectroscopic (XPS) and nuclear magnetic resonance (NMR) study, Journal of Non-Crystalline Solids 357 (2011) 170–180.

[23] S. M. Chemtob, G. R. Rossman, J. F. Stebbins, Natural hydrous amorphous silica: Quantification of network speciation and hydroxyl content by ^{29}si MAS NMR and vibrational spectroscopy, American Mineralogist 97 (2012) 203–211.

[24] A. C. Lasaga, G. V. Gibbs, Quantum mechanical potential surfaces and calculations on minerals and molecular clusters, Physics and Chemistry of Minerals 16 (1988) 29–41.

[25] W. B. De Almeida, P. J. O'Malley, The vibrational spectrum of H_4SiO_4 calculated using ab initio molecular orbital methods, Journal of Molecular Structure 246 (1991) 179–184.

[26] W. J. Malfait, V. P. Zakaznova-Herzog, W. E. Halter, Quantitative Raman spectroscopy: High-temperature speciation of potassium silicate melts, Journal of Non-Crystalline Solids 353 (2007) 4029–4042.

[27] V. P. Zakaznova-Herzog, W. J. Malfait, F. Herzog, W. E. Halter, Quantitative Raman spectroscopy: Principles and application to potassium silicate glasses, Journal of Non-Crystalline Solids 353 (2007) 4015–4028.

[28] C. T. G. Knight, J. Wang, S. D. Kinrade, Do zeolite precursor species really exist in aqueous synthesis media?, Physical Chemistry Chemical Physics 8 (2006) 3099–3103.

[29] R. A. Barrio, F. L. Galeener, E. Martinez, R. J. Elliott, Regular ring dynamics in AX_2 tetrahedral glasses, Physical Review B 48 (1993) 15672.

[30] J. D. Kubicki, D. G. Sykes, Ab initio calculation of ^{1}H, ^{17}O, ^{27}Al and ^{29}Si NMR parameters, vibrational frequencies and bonding energetics in hydrous silica and Na-aluminosilicate glasses, Geochimica et Cosmochimica Acta 68 (2004) 3909–3918.

[31] W. B. De Almeida, P. J. O'Malley, Ab initio infrared and Raman spectra of the $H_3SiO_4^-$ monomeric anionic species, Vibrational Spectroscopy 5 (1993) 325–335.

[32] J. D. Kubicki, S. E. Apitz, G. A. Blake, G2 theory calculation on $H_3SiO_4^-$, H_4SiO_4, $H_3AlO_4^{2-}$, $H_4AlO_4^-$, and H_5AlO_4: Basis set and electron correlation effects on molecular structures, atomic charges, infrared spectra, and potential energies, Physics and Chemistry of Minerals 22 (1995) 481–488.

[33] J. Sefcik, A. Goddard, Thermochemistry of silicic acid deprotonation: Comparison of gas-phase and solvated DFT calculations to experiment, Geochimica et Cosmochimica Acta 65 (2001) 4435–4443.

[34] J. D. Kubicki, D. Sykes, Molecular orbital calculations on $H_6Si_2O_7$ with a variable Si-O-Si angle: Implications of the high-pressure vibrational spectra of silicate glasses, American Mineralogist 78 (1993) 253–259.

[35] J. D. Kubicki, D. G. Sykes, Molecular orbital calculations on the vibrational spectra of $Q^3T-(OH)$ species and the hydrolysis of a three-membered aluminosilicate ring, Geochimica et Cosmochimica Acta 59 (23) (1995) 4791–4797.

[36] A. Putrino, M. Parrinello, Anharmonic Raman spectra in high-pressure ice from ab initio simulations, Physical Review Letters 88 (17) (2002) 176401.

[37] P. Umari, A. Pasquarello, A. Dal Corso, Raman scattering intensities in α-quartz: A first-principles investigation, Physical Review B 63 (2001) 094305.

[38] P. Umari, X. Gonze, A. Pasquarello, Concentration of small ring structures in vitreous silica from a first-principles analysis of the Raman spectrum, Physical Review Letters 90 (2) (2003) 027401.

[39] L. Giacomazzi, A. Pasquarello, Vibrational spectra of vitreous SiO_2 and vitreous GeO_2 from first principles, Journal of Physics: Condensed Matter 19 (2007) 415112.

[40] N. Zotov, I. Ebbsjö, D. Timpel, H. Keppler, Calculation of Raman spectra and vibrational properties of silicate glasses: Comparison between $Na_2Si_4O_9$ and SiO_2 glasses, Physical Review B 60 (1999) 6383–6397.

[41] S. Ispas, N. Zotov, S. De Wisepelere, W. Kob, Vibrational properties of a sodium tetrasilicate glass: Ab initio versus classical force fields, Journal of Non-Crystalline Solids 351 (2005) 1144–1150.

[42] Y. Liang, R. M. Caetano, S. Scandolo, Infrared and Raman spectra of silica polymorphs from an ab initio parameterized polarizable force field, The Journal of Chemical Physics 125 (2006) 194524.

[43] R. J. Heaton, P. A. Madden, Fluctuating ionic polarizabilities in the condensed phase: First-principles calculations of the Raman spectra of ionic melts, Molecular Physics 106 (2008) 1703–1719.

[44] L. Giacomazzi, P. Umari, A. Pasquarello, Medium-range structure of vitreous SiO_2 obtained through first-principles investigation of vibrational spectra, Physical Review B 79 (2009) 064202.

[45] P. Bornhauser, D. Bougeard, Intensities of the vibrational spectra of siliceous zeolites by molecular dynamics calculations. II - Raman spectra, Journal of Raman spectroscopy 32 (2001) 279–285.

[46] P. Bopp, A study of the vibrational motions of water in an aqueous $CaCl_2$ solution, Chemical Physics 106 (1986) 205–212.

[47] A. G. Kalinichev, K. Heinzinger, Molecular dynamics of supercritical water: A computer simulation of vibrational spectra with the flexible BJH potential, Geochimica et Cosmochimica Acta 59 (1995) 641–650.

[48] S. N. Taraskin, S. R. Elliott, Nature of vibrational excitations in vitreous silica, Physical Review B 56 (14) (1997) 8605–8622.

[49] M. Wilson, P. A. Madden, Polarization effects, network dynamics, and the infrared spectrum of amorphous SiO_2, Physical Review Letters 77 (16) (1996) 4023–4026.

[50] J. Sarnthein, A. Pasquarello, R. Car, Origin of the high-frequency doublet in the vibrational spectrum of vitreous SiO_2, Science 275 (1997) 1925–1927.

[51] E. A. Pavlatou, P. A. Madden, M. Wilson, The interpretation of vibrational spectra of ionic melts, Journal of Chemical Physics 107 (24) (1997) 10446–10457.

[52] M. C. C. Ribeiro, M. Wilson, P. A. Madden, On the observation of propagating sound modes at high momentum transfer in viscous liquids and glasses, Journal of Physical Chemistry 108 (21) (1998) 9027–9038.

[53] M. C. C. Ribeiro, M. Wilson, P. A. Madden, The nature of the "vibrational modes" of the network-forming liquid $ZnCl_2$, Journal of Physical Chem-

istry 109 (22) (1998) 9859–9869.

[54] M. C. C. Ribeiro, M. Wilson, P. A. Madden, Raman scattering in the network liquid $ZnCl_2$ relationship to the vibrational density of states, Journal of Physical Chemistry 110 (10) (1999) 4803–4811.

[55] M. Veithen, X. Gonze, P. Ghosez, Nonlinear optical susceptibilities, Raman efficiencies, and electro-optic tensors from first-principles density functional perturbation theory, Physical Review B 71 (2005) 125107.

[56] E. Balan, A. M. Saitta, F. Mauri, G. Calas, First-principles modeling of the infrared spectrum of kaolinite, American Mineralogist 86 (2001) 1321–1330.

[57] J. A. Tossell, Theoretical study of the dimerization of $Si(OH)_4$ in aqueous solution and its dependence on temperature and dielectric constant, Geochimica et Cosmochimica Acta 69 (2) (2005) 283–291.

[58] S. C. B. Myneni, Soft x-ray spectroscopy and spectromicroscopy studies of organic molecules in the environment., in: P. Fenter, M. Rivers, N. Sturchio, S. Sutton (Eds.), Rev. Mineral. Geochem. Applications of Synchrotron Radiation in Low-Temperature Geochemistry and Environmental Science, 2002, pp. 485–579.

[59] W. Kohn, L. J. Sham, Self-consistent equations including exchange and correlation effects, Physical Review 140 (1965) A1133–A1138.

[60] D. Marx, J. Hutter, Ab initio molecular dynamics: Theory and implementation, Modern Methods and Algorithms of Quantum Chemistry, (ed. J. Grotendorst), Forschungszentrum Jülich, NIC Series 1 (2000) 301–449.

[61] J. Perdew, K. Burke, M. Ernzerhof, Generalized gradient approximation made simple, Physical Review Letters 77 (1996) 3865.

[62] M. Pöhlmann, M. Benoit, W. Kob, First-principles molecular-dynamics simulations of a hydrous silica melt: Structural properties and hydrogen diffusion mechanism, Physical Review B (2004) 184209.

[63] R. Demichelis, B. Civalleri, P. D'Arco, R. Dovesi, Performance of 12 DFT functionals in the study of crystal systems: Al_2SiO_5 orthosilicates and Al hydroxides as a case study, International Journal of Quantum Chemistry 110 (2010) 2260–2273.

[64] D. R. Hamann, Generalized gradient theory for silica phase transitions, Physical Review Letters 76 (1996) 660–663.

[65] D. R. Hamann, Energies of strained silica rings, Physical Review B 55 (1997) 14784–14793.

[66] C. Massobrio, A. Pasquarello, R. Car, Intermediate range order and bonding character in disordered network-forming systems, Journal of the American Chemical Society 121 (1999) 2943–2944.

[67] R. M. Van Ginhoven, H. Jónsson, L. R. Corrales, Silica glass structure generation for ab initio calculations using small samples of amorphous silica, Physical Review B 71 (2005) 024208.

[68] N. Troullier, J. L. Martins, Efficient pseudopotentials for plane-wave calculations, Physical Review B 43 (1991) 1993–2006.

[69] R. Car, M. Parrinello, Unified approach for molecular dynamics and density functional theory, Physical Review Letters 55 (1985) 2471–2474.

[70] J. C. Grossman, E. Schwegler, E. W. Draeger, F. Gygi, G. Galli, Towards an assessment of the accuracy of density functional theory for first principles simulation of water, Journal of Chemical Physics 120 (2004) 300–311.

[71] E. Schwegler, J. C. Grossman, F. Gygi, G. Galli, Towards an assessment of the accuracy of density functional theory for first principles simulation of water. II, Journal of Chemical Physics 121 (2004) 5400–5409.

[72] I. F. W. Kuo, C. J. Mundy, M. J. McGrath, J. I. Siepmann, J. VandeVondele, M. Sprik, J. Hutter, B. Chen, M. L. Klein, F. Mohamed, M. Krack, M. Parrinello, Liquid water from first principles: Investigation of different sampling approaches, Journal of Physical Chemistry B 108 (2004) 12990–12998.

[73] N. P. de Koker, L. Stixrude, B. B. Karki, Thermodynamics, structure, dynamics, and freezing of Mg_2SiO_4 liquid at high pressure, Geochimica et Cosmochimica Acta 72 (2008) 1427–1441.

[74] G. J. Martyna, M. L. Klein, M. Tuckerman, Nosé-Hoover chains: The canonical ensemble via continuous dynamics, Journal of Chemical Physics 97 (1992) 2635–2643.

[75] M. P. Allen, D. J. Tildesley, Computer Simulations of Liquids, Oxford University Press, Oxford, 1987.

[76] W. Humphrey, A. Dalke, K. Schulten, VMD - Visual Molecular Dynamics, Journal of Molecular Graphics 14 (1996) 33–38.

[77] P. McMillan, A. M. Hofmeister, Infrared and Raman spectroscopy, Reviews in Mineralogy 18 (1988) 99–160.

[78] G. J. McIntosh, P. J. Swedlund, T. Söhnel, Experimental and theoretical investigations into the counter-intuitive shift in the antisymmetric ν(Si-O) vibrational modes upon deuteration of solvated silicic acid H_4SiO_4, Physical Chemistry Chemical Physics 13 (2011) 2314–2322.

[79] G. Spiekermann, M. Steele-MacInnis, P. Kowalski, C. Schmidt, S. Jahn, Vibrational properties of H_4SiO_4, $H_3SiO_4^-$ and $H_6Si_2O_7$ under various conditions from ab initio molecular dynamics, in preparation for JCP.

[80] C. Schmidt, A. Watenphul, Ammonium in aqueous fluids to 600°C, 1.3 GPa: A spectroscopic study on the effects on fluid properties, silica solubility, and K-feldspar to muscovite reactions, Geochimica et Cosmochimica Acta 74 (2010) 6852–6866.

[81] B. O. Mysen, D. Virgo, Volatiles in silicate melts at high pressure and temperature. 1. Interaction between OH groups and Si^{4+}, Al^{3+}, Ca^{2+}, Na^+ and H^+, Chemical Geology 57 (1986) 303–331.

[82] W. J. Malfait, V. P. Zakaznova-Herzog, W. E. Halter, Quantitative Raman spectroscopy: Speciation of Na-silicate glasses and melts, American Mineralogist 93 (2008) 1505–1518.

[83] I. Farnan, S. C. Kohn, R. Dupree, A study of the structural role of water in hydrous silica glass using cross-polarisation magic angle spinning NMR, Geochimica et Cosmochimica Acta 51 (1987) 2869–2873.

[84] M. Ivanda, R. Clasen, M. Hornfeck, W. Kiefer, Raman spectroscopy on SiO_2 glasses sintered from nanosized particles, Journal of Non-Crystalline Solids 322 (2003) 46–52.

[85] G. Spiekermann, M. Steele-MacInnis, P. Kowalski, C. Schmidt, S. Jahn, Vibrational properties of silica species in MgO-SiO_2 glasses using ab initio molecular dynamics, submitted to CG.